Supporting Information

The topological plasmonic chain with retardation and radiative effects

Simon R. Pocock, Xiaofei Xiao, Paloma A. Huidobro and Vincenzo Giannini

Comprised of
4 pages
2 figures
0 tables

Supporting Information: The topological plasmonic chain with retardation and radiative effects

Simon R. Pocock[†], Xiaofei Xiao[†], Paloma A. Huidobro[†], and Vincenzo Giannini[†,‡]

[†]Physics Department, Blackett Laboratory, Imperial College London, Prince Consort Road, London SW7 2AZ

[‡]Instituto de Estructura de la Materia (IEM-CSIC), Consejo Superior de Investigaciones Científicas, Serrano 121, 28006 Madrid, Spain

Lerch transcendent form

One of the challenges associated with the solving of the band structure of the infinite system is evaluating the sums in the Bloch Hamiltonian $\mathcal{G}_\nu$, given by

$$\begin{pmatrix} \sum_n' \mathrm{G}_\nu(nd,\omega)e^{ik_x nd} & \sum_n \mathrm{G}_\nu(nd+t,\omega)e^{ik_x nd} \\ \sum_n \mathrm{G}_\nu(nd-t,\omega)e^{ik_x nd} & \sum_n' \mathrm{G}_\nu(nd,\omega)e^{ik_x nd} \end{pmatrix}, \tag{1}$$

where the primed sums have $n \neq 0$. These sums exhibit poor convergence. To do this for the case of evenly spaced particles, corresponding here to the on-diagonal sums, Citrin [1] and Koenderink and Polman [2] used polylogarithms defined by the sum,

$$\mathrm{Li}_s(z) := \sum_{k=1}^{\infty} \frac{z^k}{k^s}. \tag{2}$$

These have the advantage of being implemented as standard in several scientific packages. It has been shown that we can write the on-diagonal terms in polylog form,

$$\begin{aligned} &\sum_{n\in\mathbb{Z}}{}' \mathrm{G}_x(nd)e^{ik_x nd} \\ &= \frac{2}{4\pi\epsilon_0 d^3}\Big\{\mathrm{Li}_3(e^{i(k-k_x)d}) + \mathrm{Li}_3(e^{i(k+k_x)d}) \\ &- ikd\left[\mathrm{Li}_2(e^{i(k-k_x)d}) + \mathrm{Li}_2(e^{i(k+k_x)d})\right]\Big\}, \end{aligned} \tag{3}$$

and

$$\begin{aligned} &\sum_{n\in\mathbb{Z}}{}' \mathrm{G}_{y,z}(nd)e^{ik_x nd} \\ &= -\frac{1}{4\pi\epsilon_0 d^3}\Big\{\mathrm{Li}_3(e^{i(k-k_x)d}) + \mathrm{Li}_3(e^{i(k+k_x)d}) \\ &- ikd\left[\mathrm{Li}_2(e^{i(k-k_x)d}) + \mathrm{Li}_2(e^{i(k+k_x)d})\right] \\ &- k^2d^2\left[\mathrm{Li}_1(e^{i(k-k_x)d}) + \mathrm{Li}_1(e^{i(k+k_x)d})\right]\Big\}. \end{aligned} \tag{4}$$

The off diagonal terms, with $x_n = nd \pm t$, no longer fit the form of a polylogarithm. We resort to a more general special function, the Lerch transcendent,

$$\Phi(z,s,\nu) := \sum_{k=0}^{\infty} \frac{z^k}{(k+\nu)^s}. \tag{5}$$

For our numerical calculations we make use of the fact that the Lerch transcendent can be expressed as an integral,

$$\Phi(z,s,\nu) = \frac{1}{\Gamma(s)}\int_0^{\infty} \frac{t^{s-1}e^{-\nu t}}{1-ze^{-t}}\mathrm{d}t, \tag{6}$$

where $\mathrm{Re}(\nu) > 0$, and either $|z| \leq 1, z \neq 1, \mathrm{Re}(s) > 0$ or $z = 1, \mathrm{Re}(s) > 1$ [3]. This imposes the restriction that it is not possible to calculate the Lerch transcendent on the light lines for the transverse case, as can be seen from the following equations.

The off diagonal elements in terms of the Lerch transcendent are

$$\begin{aligned} &\sum_{n\in\mathbb{Z}} \mathrm{G}_x(nd\pm t)e^{ik_x nd} \\ &= \frac{2}{4\pi\epsilon_0 d^3}\Big\{e^{ikt}\Phi\left(e^{i(k\pm k_x)d}, 3, \frac{t}{d}\right) \\ &+ e^{-ikt}e^{i(k\mp k_x)d}\Phi\left(e^{i(k\mp k_x)d}, 3, 1-\frac{t}{d}\right) \\ &- ikd\Big[e^{ikt}\Phi\left(e^{i(k\pm k_x)d}, 2, \frac{t}{d}\right) \\ &+ e^{-ikt}e^{i(k\mp k_x)d}\Phi\left(e^{i(k\mp k_x)d}, 2, 1-\frac{t}{d}\right)\Big]\Big\}, \end{aligned} \tag{7}$$

and

$$\sum_{n\in\mathbb{Z}} \mathrm{G}_{y,z}(nd\pm t)e^{ik_x nd}$$
$$= -\frac{1}{4\pi\epsilon_0 d^3}\Bigg\{e^{ikt}\Phi\left(e^{i(k\pm k_x)d},3,\frac{t}{d}\right)$$
$$+e^{-ikt}e^{i(k\mp k_x)d}\Phi\left(e^{i(k\mp k_x)d},3,1-\frac{t}{d}\right)$$
$$-ikd\Bigg[e^{ikt}\Phi\left(e^{i(k\pm k_x)d},2,\frac{t}{d}\right)$$
$$+e^{-ikt}e^{i(k\mp k_x)d}\Phi\left(e^{i(k\mp k_x)d},2,1-\frac{t}{d}\right)\Bigg]$$
$$-k^2d^2\Bigg[e^{ikt}\Phi\left(e^{i(k\pm k_x)d},1,\frac{t}{d}\right)$$
$$+e^{-ikt}e^{i(k\mp k_x)d}\Phi\left(e^{i(k\mp k_x)d},1,1-\frac{t}{d}\right)\Bigg]\Bigg\}. \quad (8)$$

Substituting $k_x = \pm\pi/d$ and $t = d/2$ we see from the above equations that

$$\sum_{n\in\mathbb{Z}} \mathrm{G}(nd\pm d/2)e^{in\pi/2} = 0, \quad (9)$$

which predicts the closing of the gap at $k_x = \pm\pi/d$, $t = d/2$ since $g_x = g_y = 0$ in equation (11) of the main text.

Trivial chiral symmetry breaking

As is the case for any 2×2 matrix, it is possible to write $\mathcal{G}$ in the form

$$\mathcal{G}(k_x) = g_0(k_x)I + \mathbf{g}(k_x)\cdot\boldsymbol{\sigma}, \quad (10)$$

where $\boldsymbol{\sigma}$ is the vector of Pauli spin matrices, and for this system in particular

$$g_0(k_x) = \sum_{n\neq0}\mathrm{G}(nd)e^{ik_x nd},$$
$$g_x(k_x) = \left[\sum_n \mathrm{G}(nd+t)e^{ik_x nd} + \sum_n \mathrm{G}(nd-t)e^{ik_x nd}\right],$$
$$g_y(k_x) = i\left[\sum_n \mathrm{G}(nd+t)e^{ik_x nd} - \sum_n \mathrm{G}(nd-t)e^{ik_x nd}\right],$$
$$g_z(k_x) = 0. \quad (11)$$

Chiral symmetry or sublattice symmetry exists when there are no interactions between sites A to A or B to B, which can be expressed in the form $\sigma_z\hat{H}\sigma_z = -\hat{H}$ [4]. This is the case when $g_0 = 0 = g_z$ in equation 10. In this model we break this chiral symmetry in a 'trivial' way. Interactions between A to A and B to B are introduced, but the A and B sublattices remain indistinguishable, because the difference between the retarded plasmonic system and a chirally symmetric system is an identity term $g_0 \neq 0$. This is important because it means that the system has the same eigenvectors as a chirally symmetric system with Bloch Hamiltonian $\mathcal{G} - g_0 I$,

$$\mathcal{G}\mathbf{p} = \frac{1}{\alpha}\mathbf{p},$$
$$(\mathcal{G} - g_0 I)\,\mathbf{p} = \left(\frac{1}{\alpha} - g_0\right)\mathbf{p}. \quad (12)$$

Since the eigenvectors are the same we can apply Zak phase results about chirally symmetric systems to our trivially non-chiral system. We also have a pseudo-chiral equation for $\mathcal{G}$ from the original chiral equation, $\sigma_z(\mathcal{G} - g_0 I)\sigma_z = -(\mathcal{G} - g_0 I)$.

This explains why the eigenvalues are not symmetric around $1/\alpha = 0$, and goes one step further:

$$(\mathcal{G} - g_0 I)\,\sigma_z\mathbf{p} = -\sigma_z\,(\mathcal{G} - g_0 I)\,\mathbf{p}$$
$$= -\left(\frac{1}{\alpha} - g_0\right)\sigma_z\mathbf{p}, \quad (13)$$

so that much like the chirally symmetric case every eigenmode $\mathbf{p}$ has a counterpart $\sigma_z\mathbf{p}$, with eigenvalues related by

$$\mathcal{G}\mathbf{p} = \frac{1}{\alpha}\mathbf{p},$$
$$\mathcal{G}\sigma_z\mathbf{p} = \left(2g_0 - \frac{1}{\alpha}\right)\sigma_z\mathbf{p}. \quad (14)$$

These equations relate the upper and lower bands of $\mathcal{G}$, although an additional non-trivial mapping is required from these eigenvalues to ω. Notably $\mathcal{G}$ also has ω dependence, which is why the eigenvalues aren't perfectly symmetric around g_0.

This can also be used to explain the fact that the edge modes of our system do not appear to be supported on only one of the sublattices, which is the case for the SSH model. Here the sublattice projection operators are given by $\hat{P}_A = (I + \sigma_z)/2$ and $\hat{P}_B = (I - \sigma_z)/2$. In the case of the fully dimerised SSH model edge modes $|\psi_n\rangle$ are zero energy $E_n = 0$, so that

$$\hat{H}\hat{P}_{A/B}|\psi_n\rangle = \hat{H}\left(|\psi_n\rangle \pm \sigma_z|\psi_n\rangle\right) = 0. \quad (15)$$

An equivalent equation for our model would be

$$\mathcal{G}\hat{P}_{A/B}\mathbf{p} = \mathcal{G}\left(\mathbf{p} \pm \sigma_z\mathbf{p}\right)$$
$$= \frac{1}{\alpha}\mathbf{p} \pm \left(2g_0 - \frac{1}{\alpha}\right)\sigma_z\mathbf{p}. \quad (16)$$

Clearly $\hat{P}_{A/B}\mathbf{p}$ is only an eigenvector of $\mathcal{G}$ when $\mathbf{p}$ and $\sigma_z\mathbf{p}$ have the same eigenvalues- which we would expect in a 'fully dimerised limit', except that such a thing does not exist due to the long range dipole-dipole interactions of the model. This suggests that the nature of the hopping makes it difficult to see a 'purely' chiral behaviour, and we can expect stronger confinement to one sublattice when $|\beta - 1|$ is larger.

It is possible to break chiral symmetry in a non-trivial way by adding a term in σ_z to the Bloch Hamilotnian, for example by changing the relative sizes of A and B particles, or making A and B different metals.

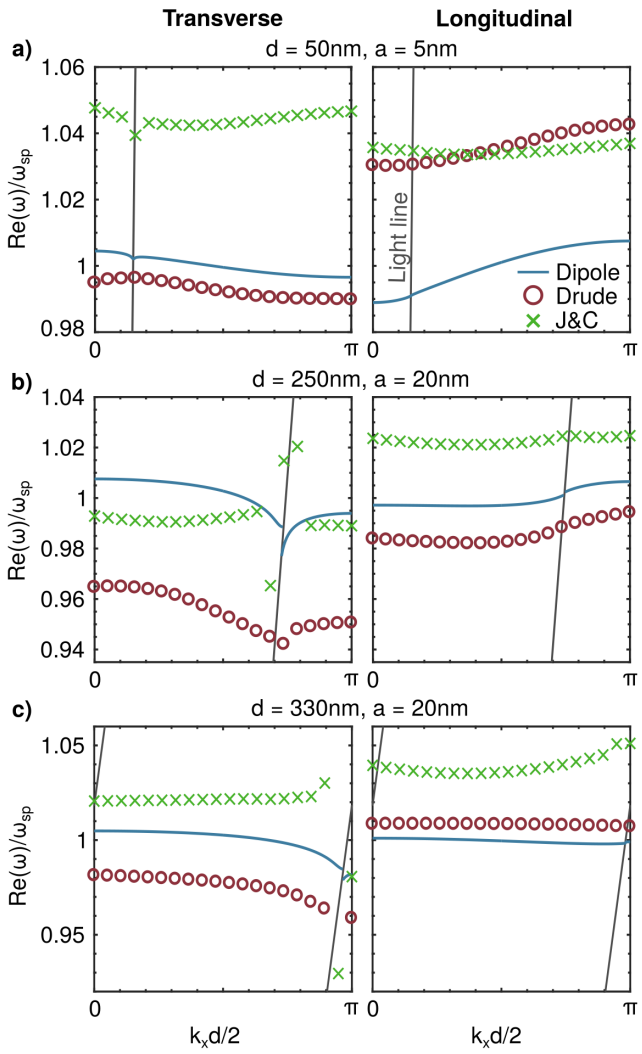

Figure S1: Comparison of coupled dipole approximation bands (blue line) with FDTD simulations using the same Drude model as in the manuscript (red circles) and experimental results from Johnson and Christy (green crosses)

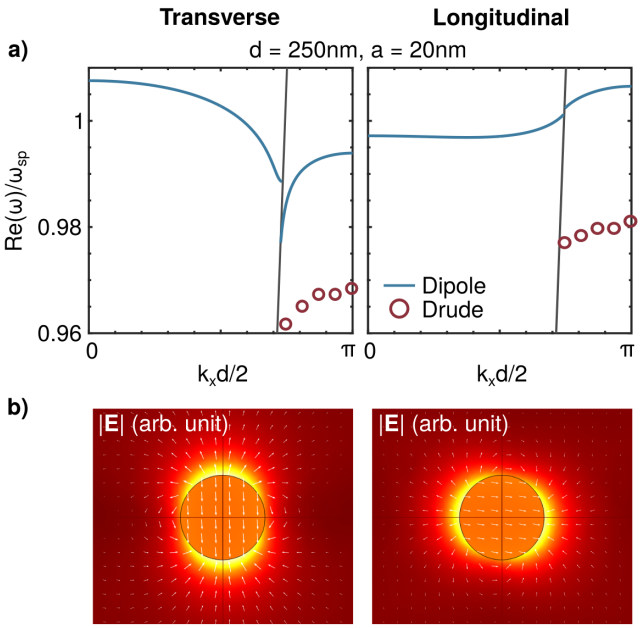

Figure S2: (a) Comparison of coupled dipole approximation bands (blue line) with FEM simulations below the light line, using the same Drude model with losses reduced by a factor of 10 (red circles). (b) Representative electric fields $|\mathbf{E}|$ of one of the modes in (a), excited by an evanescent wave. Dark red corresponds to the weakest field, and bright yellow represents a stronger field.

Full Maxwell's equations band-structures

In this section we present full Maxwell's equations simulations of the band structures of equally spaced chains, $\beta = 1$, for the d and a parameters featured in figure 2 of the main text.

In figure S1 we compare the coupled dipole approximation (CDA) (blue line) to Lumerical FDTD Solutions simulations with the same Drude model [5] (red circles), and also with experimental data for the dielectric function $\epsilon(\omega)$ of gold from Johnson and Christy [6] (green crosses). This captures the interband transitions, which are ignored in the Drude model. We consider the equally spaced chain with only a single particle per unit cell, so we only see one band in the Brillouin zone.

The comparison in figure S1 shows that the CDA (blue line) is a good approximation to the multipolar simulations, with an error smaller than 10%. When the Drude model is used (red circles) there is a small shift but a similar band shape is recovered, featuring evidence of polariton-like behaviour at the light line. The inclusion of the full experimental dielectric function (green crosses) changes the shape of the bands more dramatically due to the presence of interband transitions, although this should not have an effect on the qualitative topological properties of the system. The inclusion of a different dielectric function changes the polarisability of the particles $\alpha(\omega)$, but does not change whether gaps close, which is dictated by the zeros of the off diagonals of the Hamiltonian matrix in equation 1. As explained in the discussion of figure 4 in the main text, a different polarisability can shift band crossings in the d parameter, but doesn't change whether band crossings exist or not.

For figure S1 an FDTD solver (Lumerical) was used to search the eigenfrequencies by placing a number of randomly oriented and randomly distributed dipole sources to excite all modes of interest for the system. A cloud of randomly distributed time monitors was applied to obtain a spectrum with peaks at the resonant frequencies using the Fourier transform of the time signal. By running a parameter sweep over a range of the Bloch vectors and finding the local maxima of the spectrum for each Bloch vector, the band structure can be found [7]. However, according to the Lumerical webpage regarding simulations with loss, 'the fields decay more quickly when more loss is introduced, and the useful part of the time signal that is collected by the time monitors is shortened. The Fourier transform of the time signal becomes noisy, making it difficult to extract the resonance peaks' [8]. Therefore special settings need to be chosen to excite the interesting modes and make the bands more visible. In our simulation we also used

symmetry or antisymmetry on the y and z axes to isolate the longitudinal and transverse modes.

In figure S2(a) we compare the coupled dipole approximation (CDA) (blue line) to Comsol FEM simulations with the same Drude model with losses reduced by a factor of 10 [5] (red circles). In the simulation an evanescent wave is incident on the chain, and peaks in absorption are used to construct the bands below the light line. Reduced losses help to resolve these peaks. Unlike the messy incident fields created by dipole clouds in the previous method, evanescent waves allow us to clearly see the near fields of the particles at the modes. Example near fields in the xy plane are shown in figure S2(b), where colour shows the magnitude of the field $|\mathbf{E}|$ and white arrows the direction and size of the field. These modes are represented well by transverse and longitudinal dipoles.

There are some limitations to these approaches to calculating the band structures, as Lumerical struggles with simulations featuring lossy systems like this one, and it is difficult for Comsol to solve for eigenmodes with the combination of open and periodic boundary conditions required to find band structures of a chain of $3D$ particles.

References

[1] D. S. Citrin. Plasmon-polariton transport in metal-nanoparticle chains embedded in a gain medium. *Opt. Lett.*, 31(1):98–100, 2006.

[2] A. Femius Koenderink and Albert Polman. Complex response and polariton-like dispersion splitting in periodic metal nanoparticle chains. *Phys. Rev. B*, 74:033402, 2006.

[3] I. S. Gradshteyn, I. M. Ryzhik, A. Jeffrey, and D. Zwillinger. *Table of Integrals, Series and Products, 7th edition*. Academic Press, US, 2007.

[4] János K. Asbóth, László Oroszlány, and András Pályi. *A Short Course of Topological Insulators*. Springer International Publishing, Switzerland, 2016.

[5] Alexandre Vial, Anne-Sophie Grimault, Demetrui Macias, Dominique Barchiesi, and Marc Lamy de la Chapelle. Improved analytical fit of gold dispersion: Application to the modeling of extinction spectra with a finite-difference time-domain method. *Phys. Rev. B*, 71:085416, 2005.

[6] P. B. Johnson and R. W. Christy. Optical constants of the noble metals. *Phys. Rev. B*, 6:4370–4379, Dec 1972.

[7] Lumerical Inc. Simulation methodology, 2018. `https://kb.lumerical.com/en/index.html?diffractive_optics_pc_simulation_methodology.html` [accessed 10-April-2018].

[8] Lumerical Inc. Simulations with loss, 2018. `https://kb.lumerical.com/en/diffractive_optics_pc_simulations_with_loss.html` [accessed 4-April-2018].